ELSEVIER

Journal of Alloys and Compounds 235 (1996) 150–155

Journal of ALLOYS AND COMPOUNDS

# Synthesis and characterization of fine particle $ZnFe_2O_4$ powders by a low temperature method

Xinyong Li, Gongxuan Lu, Shuben Li

*State Key Laboratory for Oxo Synthesis and Selective Oxidation, Lanzhou Institute of Chemical Physics, Chinese Academy of Sciences, Lanzhou, 730000, People's Republic of China*

Received 10 June 1995; in final form 5 August 1995

**Abstract**

Fine particle $ZnFe_2O_4$ powders have been prepared by the low temperature process without any intermediate phase formation. The precursor was prepared and fired at low temperature to form the desired product. Very pure, fine, monophase $ZnFe_2O_4$ powders were obtained by the calcination of the precursor in air to about 450°C for 2 h. The IR and EPR characteristics of the fine powders are presented and discussed in terms of the particle size effect.

*Keywords:* Zinc ferrite; Fine particle; Low temperature method; FT–IR; EPR

## 1. Introduction

Zinc ferrite currently receives enormous scientific attention owing to its superior catalytic activity [1–3] and interesting magnetic characteristics [4,5]. Several procedures have been employed to prepare $ZnFe_2O_4$ powders, including solid-state reactions [5,6], co-precipitation methods [7], in which the reaction temperature is high (1300°C) and controlling the particle size is not easy.

In this paper, we have tried to prepare $ZnFe_2O_4$ fine particles at low temperature. Thereafter, the crystal structure, particle morphology, IR and EPR characteristics of $ZnFe_2O_4$ powders have been investigated.

## 2. Experimental details

### 2.1. Powder preparation

Zn and Fe nitrates (A.R) in a 1:2 molar ratio of cations were dissolved together in a minimum amount of deionized water, to produce a clear solution. Polyvinyl alcohol (PVA: polymerization degree was 2000) was used to make a gel. The aqueous PVA solution was added to the nitrate solution and dehydrated at 60–80°C. The gelation proceeded step by step and a slightly red gel-type precursor was obtained. The precursor was then calcined at 450–650°C for 2 h in air to obtain $ZnFe_2O_4$ fine powders. The thermal decomposition behavior of the precursor was investigated by using thermogravimetry (TG) and differential thermal analysis (DTA) (Dupant 9900) in air at a heating rate of 10°C $min^{-1}$. The crystalline structure of the samples was identified from the X-ray diffraction patterns taken on a Ragaku/D/max – $\gamma$ B diffractometer using Cu K$\alpha$ radiation. Particle size and morphology were observed by transmission electron microscopy (JEM-1200EX/S). The FT–IR spectrum was also employed to identify the chemical composition and phases by using a Nicolet 10DX Fourier transform infrared spectrometer. The electron paramagnetic resonance (EPR) technique was performed to examine the EPR characteristics of $ZnFe_2O_4$ samples calcined at different temperatures. EPR spectra were recorded at room temperature with a varin E-115 spectrometer operating in the X-band ($u = 9.2$ GHz) with 100 kHz field modulation. EPR parameters were calibrated by comparison with a standard $Mn^{2+}$–ZnS (1–6 line distance, 34.05 mT) and 2,2-diphenyl-1-picrylhydrazyl (DPPH, $9.7 \times 10^{15}$ spins, $g = 2.0036$).


*SSDI* 0925-8388(95)02022-5

## 3. Results and discussion

### 3.1. The thermal decomposition behavior of the gel-type precursor

Fig. 1 shows the TG and DTA curves for the gel-type precursor. At first, a slight weight loss below 250°C in the TG curve might be attributed to the liberation of surface adsorbed water or other substances such as free nitric acid. Subsequently, a strong exothermic peak in the DTA curve with drastic weight loss is observed in the temperature range 250–500°C, which corresponds to the conventional oxidative decomposition of PVA-based phases as well as nitrates [8]. Afterwards, corresponding to the TG curve, the exothermicity of the redox reaction between PVA and metal nitrates in fact has completed at 500°C, indicating the completion of PVA-chain and nitrates decomposition.

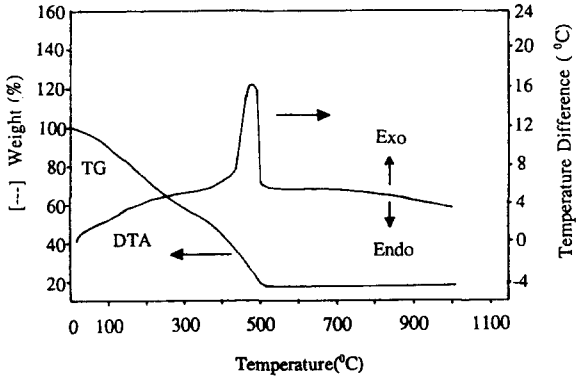


Fig. 1. TG–DTA curves of the gel-type precursor for zinc ferrite fine particles, heating rate: 10°C $min^{-1}$ in air.

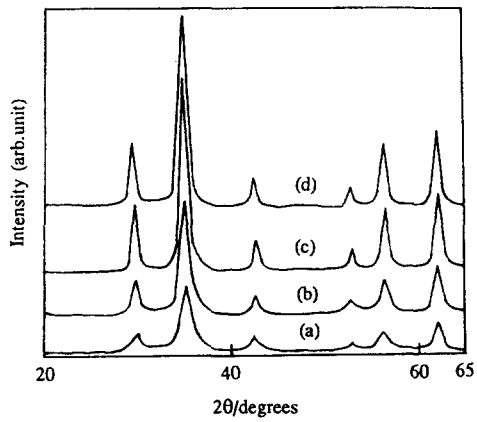


Fig. 2. X-ray diffraction patterns of $ZnFe_2O_4$ samples calcined at different temperatures for 2 h followed by slow cooling: (a) 450°C, (b) 500°C, (c) 600°C, (d) 650°C.

The X-ray diffraction patterns of samples calcined at different temperatures are shown in Fig. 2. It is evident that in all cases the spinel phase could be produced at rather low temperature compared to the conventional solid-ceramic techniques (1300°C) and the diffraction peaks are fairly broad, particularly for the lower temperature. The peak broadening may be caused by the small particle size and the interface structure with a large volume fraction and without any order [9]. The six broad peaks, centered at $2\theta =$ 29.86°, 35.16°, 42.78°, 52.96°, 56.58° and 62.26°, respectively, match well with the $ZnFe_2O_4$ crystal faces [220] ($d_1 = 2.986$ Å), [311] ($d_2 = 2.550$ Å), [400] ($d_3 =$ 2.109 Å), [422] ($d_4 = 1.728$ Å), [511] ($d_5 = 1.625$ Å), [440] ($d_6 = 1.486$ Å), respectively.

Particle sizes of the zinc ferrite samples as calculated from Scherrer's formula are shown in Table 1. It is evident that the crystallite size of the ferrite phase as obtained in the present investigation varies from 6.7 nm to 13.9 nm, depending on the calcination temperature, which is fairly consistent with the particle size determined by transmission electron microscopy (TEM).

From Fig. 2, it may be noticed that no change in the crystal structure occurs in the XRD patterns of the powders. The only effect is that the X-ray line broadening gradually decreases with increasing calcination temperature, which is due to the grain growth of the large crystallites at higher temperatures (see Table 1).

Isothermal heating of the gel-type precursor was also carried out in flowing nitrogen and argon atmospheres, to check the effect of atmosphere (oxygen partial pressure) on the formation of $ZnFe_2O_4$. It was found that the formation of $ZnFe_2O_4$ was not affected by the surrounding atmosphere. Thus, the minimum calcination temperature for the formation of pure crystalline $ZnFe_2O_4$ phase was found to be around 450°C, which is 800–900°C lower than the temperature

Table 1
Heat treatment schedule and particle size in $ZnFe_2O_4$ fine particles

| Sample No. | Calcination temperature (°C) | Particle size (nm) | Colour |
|---|---|---|---|
| 1 | 450 | 6.7 | light-red |
| 2 | 500 | 8.5 | brown-red |
| 3 | 600 | 12.7 | brown-red |
| 4 | 650 | 13.9 | dark-red |

employed in conventional ceramic processing methods [5]. The lower formation temperature of $ZnFe_2O_4$ was ascribed to the greater reactivity of the homogeneously dispersed PVA-based precursor powders employed.

### 3.2. Electron microscopy and particle size

Fig. 3(a)–(d) shows the transmission electron micrograph (TEM) of the samples of $ZnFe_2O_4$ calcined

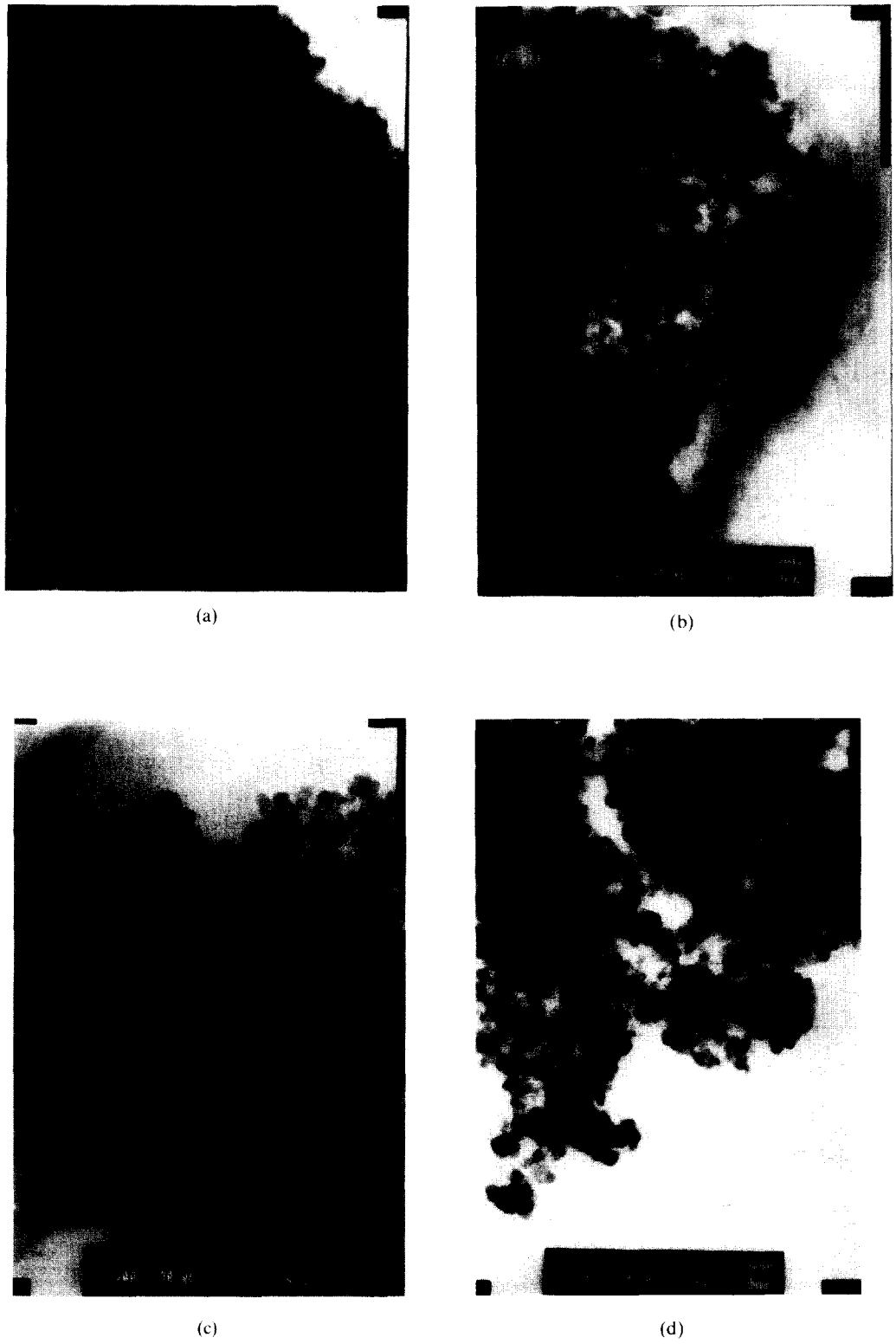


Fig. 3. Transmission electron micrograph for samples calcined at (a) 450°C, (b) 500°C, (c) 600°C and (d) 650°C.

at 450°C, 500°C, 600°C, and 650°C. A progressive change in morphology is evident with increased calcination temperature. The zinc ferrite powders calcined at 450°C were fine, of uniform size and spherical. The average grain sizes increased with the calcination temperature and the grain became blocky.

The selected area diffraction (SAD) pattern of the calcined powder at 450°C is shown in Fig. 4. It is easily seen that the characteristic $ZnFe_2O_4$ rings are fairly diffused, which also confirms the small size of the particles, whereas the selected area diffraction patterns of the other two samples were much more distinct, which shows that the size of the particles increases with increasing calcination temperature.

### 3.3. Infrared spectroscopy

Fig. 5 shows the FT–IR spectrum of samples calcined at different temperatures.

It can be observed from this figure that the $ZnFe_2O_4$ fine powders not only exhibit four IR-active bands (two at higher frequencies and the other two at low frequencies), designated $v_1$, $v_2$, $v_3$ and $v_4$, but also some shoulders. The first two higher frequency bands are assigned to stretching vibrations due to interactions produced between the oxygen and the cations occupying the octahedral and tetrahedral sites. The band around 330 $cm^{-1}$ frequency ($v_3$ mode) is attributed to displacement of the tetrahedral cations by the octahedral cations, while the fourth one is due to some

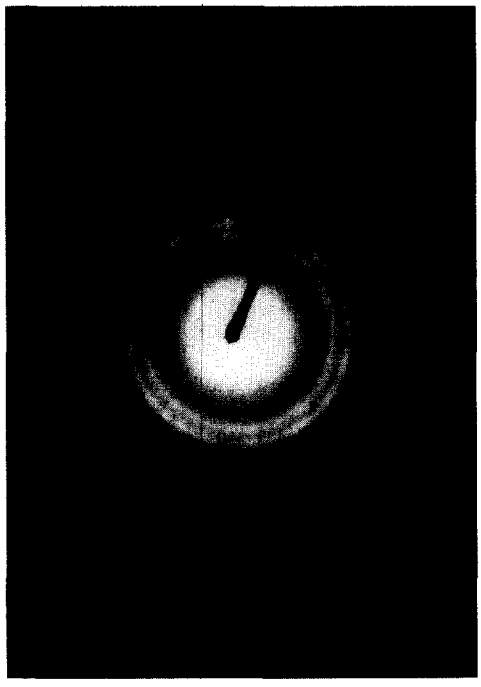

Fig. 4. Selected area diffraction pattern of sample calcined at 450°C for 2 h followed by slow cooling.

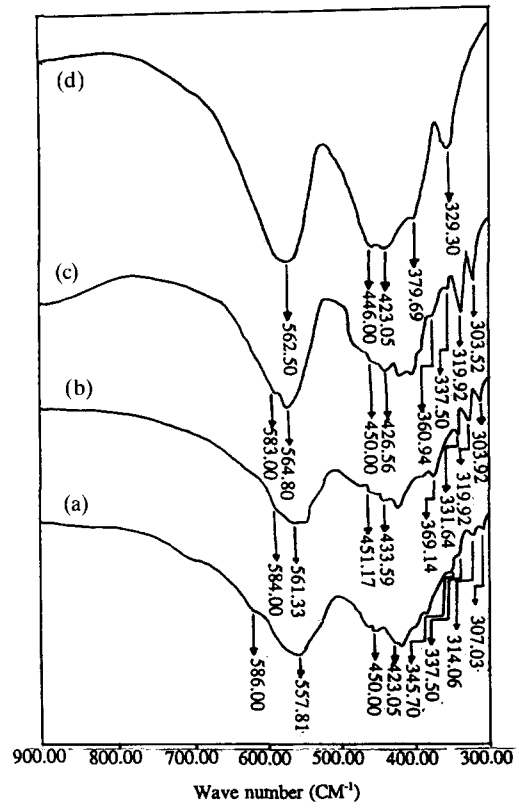


Fig. 5. FT–IR spectrum of samples calcined at (a) 450°C, (b) 500°C, (c) 600°C and (d) 650°C.

type of lattice vibrations [10]. The shoulders corresponding to 1st, 2nd, 3rd and 4th principal bands are designated $v_{1s}$, $v_{2s}$, $v_{3s}$, and $v_{4s}$, respectively. The positions of all bands together with their shoulders are summarized in Table 2. The occurrence of the shoulders is attributed to the splittings of the bands, whereas the splittings may be attributed to Jahn–Teller distortion [11] produced by $Fe^{3+}$ ions which locally produces deformation in the lattice owing to a monocubic component of the crystal field potential. On the other hand, the symmetry of the fine $ZnFe_2O_4$ powders gradually decreased with decreasing particle sizes, and this can also induce the four principal IR bands to split more shoulders.

### 3.4. EPR spectra of $ZnFe_2O_4$ fine particles

The EPR spectra of $ZnFe_2O_4$ fine powders have been recorded at room temperature. A typical EPR spectrum is shown in Fig. 6. It can be observed that the EPR spectra shows a single broad signal with a $g$ value of around 2.006, which is attributed to the paramagnetic centers, i.e. $Fe^{3+}$. Furthermore, we performed quantitative EPR measurements and the results are shown in Table 3. It is concluded that the EPR parameters (i.e. the line width (ΔHpp) and the spin number) show a size and temperature depen-

Table 2
FT-IR band positions of zinc ferrite fine particles ($cm^{-1}$)

| Sample No. | $v_1$ | $v_{1s}$ | $v_2$ | $v_{2s}$ | $v_3$ | $v_{3s}$ | $v_4$ | $v_{4s}$ |
|---|---|---|---|---|---|---|---|---|
| 1 | 577.81 | 586.00 | 423.05 | 450.00 | 337.50 | 345.70 | 314.06 | 307.03 |
| 2 | 561.33 | 584.00 | 433.59 | 451.17 | 331.64 | 369.14 | 319.92 | 303.92 |
| 3 | 564.80 | 583.00 | 426.56 | 450.00 | 337.50 | 360.94 | 319.92 | 303.52 |
| 4 | 562.50 | – | 423.05 | 446.00 | 329.30 | 379.69 | – | – |

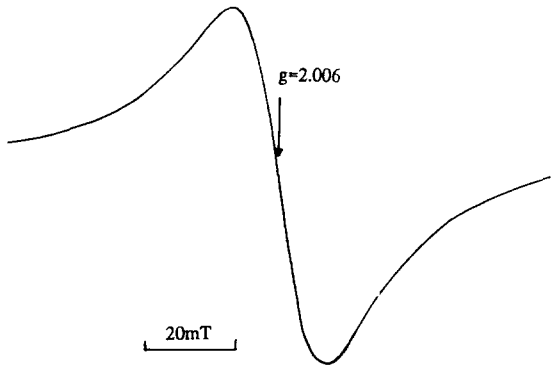


Fig. 6. Electron paramagnetic resonance spectra of sample 1 taken at room temperature.

dence. When the calcination temperature is below 600°C, the EPR parameters increased with increasing calcination temperature and particle size, whereas they were reversible with further increases in the calcination temperature and particle size. For the former, the reason may be ascribed to the increased crystallization degree of $ZnFe_2O_4$ fine particles with increasing calcination temperature and particle size as revealed by XRD techniques. This could make the spin number of $Fe^{3+}$ increase and the interaction among the paramagnetic centers increase. Therefore, the EPR parameters increased with increasing calcination temperature and particle size.

When the calcination temperature is above 600°C, some agglomerization occurs among $ZnFe_2O_4$ fine particles as revealed by TEM and this tendency increases with further increases in the calcination temperature and particle sizes. The EPR technique may not detect the agglomerated $Fe^{3+}$, which could be called "EPR invisible $Fe^{3+}$" which is similar to "EPR invisible $O^-$" proposed by Boudart et al. [12]. Thus, the spin number decreased along with the decreasing of ΔHpp. However, the exact mechanism remains unclear.

## 4. Conclusions

The low temperature process has been successfully employed for the preparation of fine $ZnFe_2O_4$ particles at a temperature 800–900°C lower than that required by the conventional solid ceramic method. The powder obtained by this method is chemically homogeneous and fine and consequently this process is very useful for the low temperature preparation of $ZnFe_2O_4$ and related oxides. The morphology and crystal structure of the particles were investigated with TEM and XRD techniques. The IR and EPR characteristics for fine particles are presented and discussed in terms of the particle size effect.

## Acknowledgements

This work was supported by the National Natural Science Foundation of China.

## References

[1] L.M. Welch, L.J. Croce and H.F. Christmann, *Hydro. Proc., 57* (1978) 131.
[2] H.H. Kung and M.C. Kung, *Adv. Catal., 33* (1985) 159.
[3] W.Y. Zhou, X.C. Cheng and Q.Y. Li, *Cui Hua Xue Bao (in Chinese), 8* (1987) 121.
[4] T. Sato, K. Haneda, M. Seki and T. Iijima, *Appl, Phys. A., 50* (1990) 13.
[5] H. Hibst, U.S. Patent 4 425 250, 1984.

Table 3
Heat treatment schedule and EPR characteristics in different $ZnFe_2O_4$ fine particles

| Sample No. | Calcination temperature (°C) | Particle size (nm) | Line width ΔHpp (mT) | Spin number ($\times 10^{22}$ spins $g^{-1}$) |
|---|---|---|---|---|
| 1 | 450 | 6.7 | 22 | 63 |
| 2 | 500 | 8.5 | 28 | 84 |
| 3 | 600 | 12.7 | 35 | 123 |
| 4 | 650 | 13.9 | 30 | 114 |

[6] Y. Hayashi, T.Kimura and T. Yamaguchi, *J. Mater. Sci., 21* (1986) 2876.
[7] Gongxuan Lu, *Ph.D. Thesis*, Lanzhou Institute of Chemical Physics, Chinese Academy of Sciences, 1993.
[8] Huayang, Lizhou Song, Fengqing Wu and Zichen Wang, *J. Mater. Sci. Lett., 13* (1994) 256.
[9] X. Zhu, U. Birringer and H. Gleiter, *Phys. Rev., B35* (1987) 9085.
[10] J. Preudhomme and P. Tarte, *Spectrochim. Acta., 27A* (1971) 961.
[11] O.S. Josyulu and J. Sobhanadri, *Phys. Stat. Solidi (a)., 65* (1981) 479.
[12] M. Boudart, A.J. Delbouille, E.G. Derouane, V. Indovino, and A.B.J. Walters, *J. Am. Chem. Soc., 94* (1972) 6622.